Available online at www.sciencedirect.com
SCIENCE DIRECT®
Journal of Catalysis 220 (2003) 333–346
JOURNAL OF CATALYSIS
www.elsevier.com/locate/jcat

DFT study on the electrophilic aromatic substitution catalyzed by Lewis acids

Ann M. Vos,[a,*] Robert A. Schoonheydt,[a] Frank De Proft,[b] and Paul Geerlings [b]

[a] *Center for Surface Chemistry and Catalysis, Katholieke Universiteit Leuven, Kasteelpark Arenberg 23, 3001 Leuven, Belgium*
[b] *Eenheid Algemene Chemie, Vrije Universiteit Brussel, Pleinlaan 2, 1050 Brussel, Belgium*

Received 13 March 2003; revised 20 June 2003; accepted 9 July 2003

Abstract

The reaction mechanisms of the H-exchange and methylation of benzene catalyzed by various Lewis acid catalysts are investigated through DFT calculations. The reactions are concerted and no stable charged intermediates are formed. Reaction rate constants and HSAB-based reactivity descriptors are calculated to compare the activity of the different Lewis acids. $AlCl_3$ is always more active than BF_3, in agreement with experimental results. The ranking of $Al(OH)_3$ and the L_1 site of zeolites, which have comparable active centers, in this activity sequence is less obvious. $\Sigma(\Delta s_{AB})^2$ values appear to be a good reactivity descriptor for describing the intermolecular reactivity sequences of these reactions.

Keywords: Lewis acidity; Zeolites; Methylation of benzene; H-exchange of benzene; DFT; Reaction rate constants; HSAB; Local softness; Local hardness

1. Introduction

The Friedel–Crafts alkylation is the most famous example of an acid-catalyzed electrophilic aromatic substitution reaction. Traditionally, homogeneous Lewis acids, like $AlCl_3$ or BF_3, are used as catalyst, but homogeneous Brønsted acids like H_2SO_4 can also catalyze the reaction [1]. Furthermore this reaction can be catalyzed by environmentally more friendly solid acid catalysts, like zeolites [2]. When acid zeolites are used, it is not entirely clear whether the bridging hydroxyl groups are the sole reaction centers or whether there are also Lewis acid sites involved.

Steaming of zeolites results in dealumination of the zeolite framework and the formation of a variety of extraframework Al species [3]. These extraframework Al species are possible electron acceptors or Lewis acids. The exact nature of these Lewis sites is still not fully understood but possibly tri- or penta-coordinated Al species are involved [4]. In catalysis these Al species appear to play an important role, but the exact role of the Lewis acid sites is still a matter of debate. According to Biaglow et al. [5] and Sohn et al. [6] there exists a synergy between the Brønsted acid sites or bridging hydroxyl groups and the Lewis acid sites. The Lewis acid sites are believed to polarize nearby bridging hydroxyl groups, thus enhancing their catalytic activity. On the other hand, Schoofs et al. [7] explained their results for the H/D-exchange of isobutane by assuming initiation of the reaction by hydride extraction on Lewis acid sites, thus proposing Lewis acid sites to be involved directly in catalysis.

Theoretical studies of the catalytic activity of Lewis acid sites in zeolites are, in contrast with those of Brønsted acid sites [8–13], rather rare. Some attempts were made to model the interaction of Lewis acid site with probe molecules like CO by Pelmenschikov et al. [14], Bates and Dwyer [15], and Neyman et al. [16]. Recently ab initio molecular dynamics simulations have been performed to study the structural properties of $Al(OH)_3(H_2O)$ and $Al(OH)_3(H_2O)_3$ particles inside the zeolite framework [17]. As there is very little known about the structure of Lewis acid sites, all these studies assumed $Al(OH)_3(H_2O)_x$ systems, with x varying between 0 and 3, to represent the Lewis acid sites. Lamberov et al. [18] used AM1 calculations to study the dealumination process of high-siliceous zeolites. They found theoretical evidence for a possible pathway for generating Lewis acid sites. Their Lewis acid sites consist of tri-coordinated Al as can be seen in Fig. 1. The L_1 site appears to be the strongest

* Corresponding author.
E-mail address: ann.vos@agr.kuleuven.ac.be (A.M. Vos).

0021-9517/$ – see front matter
doi:10.1016/S0021-9517(03)00310-5

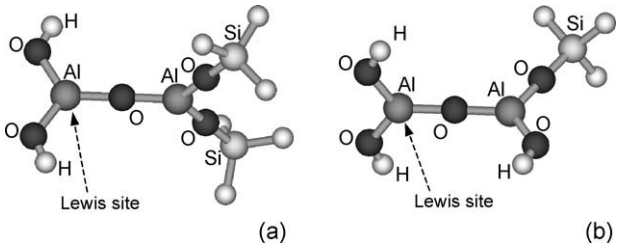

Fig. 1. Lewis acid sites according to Lamberov et al. [18] (a) L_1 site, (b) L_2 site. The Si atoms are terminated by H atoms. In reality they belong to the zeolite lattice. Thus, H atoms replace the remainder of the zeolite lattice.

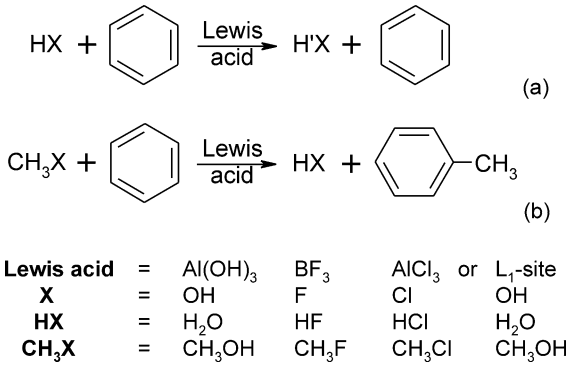

Fig. 2. Scheme of the studied reactions.

Lewis acid, though they could not exclude the existence of other, stronger Lewis acid sites.

In this work we investigated the reaction mechanism of simple electrophilic aromatic substitution reactions, namely, H-exchange and methylation, catalyzed by Lewis acids. Both traditional homogeneous Lewis acids, BF_3 and $AlCl_3$, and the Lewis acid sites in zeolites are investigated (see Fig. 2).

2. Method

2.1. Geometry optimizations

The geometry of reactants, transition structures, and products are optimized with Gaussian 98 [19] using a B3LYP exchange-correlation functional [20,21]. Because Otto [22] has demonstrated that diffuse functions are necessary for describing the weak interaction bond between B and F correctly, a 6-31+G** basisset is used for these and all other systems. The cluster used to represent the Lewis acid site in zeolites is given in Fig. 1a. To preserve electrical neutrality, dangling bonds are saturated with hydrogen atoms. After geometry optimization, reaction rate constants and DFT-based reactivity descriptors are calculated [23–25].

The complete reaction path (intrinsic reaction coordinate or IRC) of the reactions has been calculated at the AM1 level [26], using GAMESS [27]. First the transition structure was optimized at the AM1 level and from this transition structure, the IRC was reconstructed by following the steepest descent path using the Gonzalez–Schlegel second-order method toward reactants at one side and products at the other side [28,29]. The AM1 level of calculation is the result of balancing the cost of IRC calculations and the quality of the obtained structures. As shown in Section 3, the structures obtained by AM1 calculations resemble those obtained by B3LYP/6-31+G** close enough to give the same general picture of the course of the reactions studied here.

2.2. Calculation of reaction rate constants

The reaction rate constants, k_r, have been calculated within the framework of Eyring's transition state theory as [30–32]

$$k_r = (N_A V)^{i-1}\left(\frac{RT}{N_A h}\right)\frac{Q^{++}}{\prod_i Q_i}e^{-E_{act}/RT}, \quad (1)$$

with N_A Avogadro's number, V the molar volume, h the constant of Planck, R the universal gas constant, and T the temperature. E_{act}, the activation energy of the reaction, equals the energy difference between reactants and transition state and contains the zero point energy corrections. The molecular partition functions of the transition state (Q^{++}) and of the i reactants (Q_i) are evaluated using a rigid rotor harmonic oscillator approximation under the assumption that rotational, vibrational, and electronic movements are independent of each other.

The rate constants were calculated for a temperature ranging from 300 to 800 K with partition functions obtained after a vibrational analysis by Gaussian 98 [19] (B3LYP/6-31+G**), where the frequencies were scaled according to the procedure proposed by Scott and Radom [33].

When these kinetic data are analyzed in terms of an Arrhenius expression [30] by plotting $\ln(k_r)$ against T^{-1} and fitting a straight line through it, the Arrhenius activation energy (E_{Arr}) and the preexponential factor (A) are obtained

$$\ln k_r = \ln A - \frac{E_{Arr}}{RT}. \quad (2)$$

The preexponential factor (A) is proportional to the entropy difference between reactants and transition state (ΔS_{act}) [32],

$$\Delta S_{act} = R\left[\ln A - \ln\left(\frac{k_B T}{h}\right) - (1-\Delta n) + \ln V^{\Delta n}\right], \quad (3)$$

with Δn the change in the number of molecules from the reactants to the transition state.

2.3. Calculation of density functional-based reactivity descriptors

In 1963, the term "hard and soft acids and bases" (HSAB) was introduced by Pearson, to enable a better description of the interaction between Lewis acids and bases [34]. Hard acids prefer to coordinate to hard bases and soft acids prefer to coordinate to soft bases. Hard–hard combinations result

mainly in ionic bonds whereas soft–soft combinations result in covalent bonds. With the application of density functional theory (DFT) to chemical systems, it became possible to define sharply and to quantify the—until then rather intuitive—concepts of hardness and softness [35–40].

Within this conceptual branch of DFT the global hardness (η) is defined as the second derivative of the energy (E) with respect to the number of electrons (N) at constant external potential ($v(\mathbf{r})$) [41]

$$\eta = \frac{1}{2}\left(\frac{\partial^2 E}{\partial N^2}\right)_{v(\mathbf{r})} = \frac{1}{2S}, \tag{4}$$

where S is the global softness. In the finite difference approach η can be written as

$$\eta = \frac{IE - EA}{2}, \tag{5}$$

with IE and EA the first vertical ionization energy and the electron affinity of the molecule. In the frozen core approximation, η equals the HOMO–LUMO gap

$$\eta = \frac{E_{\mathrm{LUMO}} - E_{\mathrm{HOMO}}}{2}. \tag{6}$$

The HSAB principle is not only valid at the molecular level, but also at the local level (atoms, functional groups); for example, soft atoms react preferentially with other soft atoms and hard atoms react preferentially with other hard atoms [42–45].

The atomic softness can be calculated as [46]

$$s_k^i = f_k^i \cdot S \quad \text{with } i = + \text{ or } -, \tag{7}$$

where f_k^i is the atomic Fukui function. f_k^- is an index describing the reactivity toward an electrophilic attack, while f_k^+ describes the reactivity toward a nucleophilic attack [47,48]. f_k^- and f_k^+ are evaluated using atomic populations (q_k) [49]

$$f_k^+ = \left[q_k(N+1) - q_k(N)\right], \tag{8}$$

$$f_k^- = \left[q_k(N) - q_k(N-1)\right] \tag{9}$$

and the atomic charges are obtained using a natural population analysis (NPA) [50] in Gaussian 98 [19] (B3LYP/6-31+G**).

The local HSAB principle has often been used invoking softness matching through calculation of the difference in atomic softness between an electrophilic atom A and a nucleophilic atom B [42–45]

$$\Delta s_{\mathrm{AB}} = \left|s_{\mathrm{A}}^- - s_{\mathrm{B}}^+\right|. \tag{10}$$

For orbital controlled reactions, the difference in atomic softness (Δs_{AB}) should be as small as possible to promote the reaction. By analogy one could propose that for a charge controlled reaction the difference in atomic hardness ($\Delta\eta_{\mathrm{AB}}$) of the two interacting atoms A and B should be as small as possible [24,25].

However, the definition of the local hardness is ambiguous [51–55] and the same is true for any condensed version of the local hardness. Nevertheless, we are interested in using a quantity for describing hard–hard or charge controlled interactions as a counterpart of the atomic softness [56]. In the original definition of hard and soft acids and bases, a hard acid has an acceptor atom with high positive charge. Therefore, the atomic charge is used here as a measure for the local hardness, as they both quantify essentially the reactivity in charge controlled reactions or reaction steps. In this work NPA charges [50] are used as an approximation for the condensed local hardness

$$\eta_k \approx |q_k|. \tag{11}$$

Obviously, the actual values q_k are dependent on the method used; however, trends obtained with the method and basis set used in this work can be expected to remain unaltered whatever the method or basis set.

For interaction complexes with more then one interaction center none of the calculated local reactivity descriptors on its own can take into account all the interactions that are important. Therefore, following the approach of Pal and coworkers [57] and the present authors [43], a sum of squares of the Δs_{AB} values was calculated, $\Sigma(\Delta s_{\mathrm{AB}})^2$, with A and B being any pair of atoms that interact with each other. By analogy also the sum of squares of the $\Delta\eta_{\mathrm{AB}}$ values was calculated, $\Sigma(\Delta\eta_{\mathrm{AB}})^2$.

The $\Sigma(\Delta s_{\mathrm{AB}})^2$ value and/or $\Sigma(\Delta\eta_{\mathrm{AB}})^2$ value should be as small as possible to promote the reaction.

3. Results and discussion of the geometry optimizations

3.1. Overview of the molecules involved in the reactions

Four different models for Lewis acid catalysts were used in this study: $Al(OH)_3$, BF_3, and $AlCl_3$ as examples of traditional homogeneous catalysts and a cluster to represent a Lewis acid site (L_1 site) inside a zeolite. For the H-exchange reaction these Lewis acids are used in combination with, respectively, H_2O, HF, HCl, and H_2O (see Fig. 2). These molecules provide the proton necessary for the H-exchange reaction. For the methylation of benzene, the Lewis acids are used in combination with respectively CH_3OH, CH_3F, CH_3Cl, and CH_3OH as methyl-donating molecules (see Fig. 2).

In Fig. 3, a general scheme for these reactions is given. The molecules first have to approach each other to form a Lewis acid–HX–benzene complex (for H-exchange) and Lewis acid–CH_3X–benzene complex (for methylation). We also studied the Lewis acid–HX and Lewis acid–CH_3X complexes without benzene to get information about the interactions between the Lewis acid and HX or CH_3X, respectively. The geometry of all the structures are given in Fig. 4. The structures are symbolized by the following letter code: **r**, **ts**, or **p** for reactants, transition structures, or products, respectively, and **H** or **M** for structures involved in the H-exchange

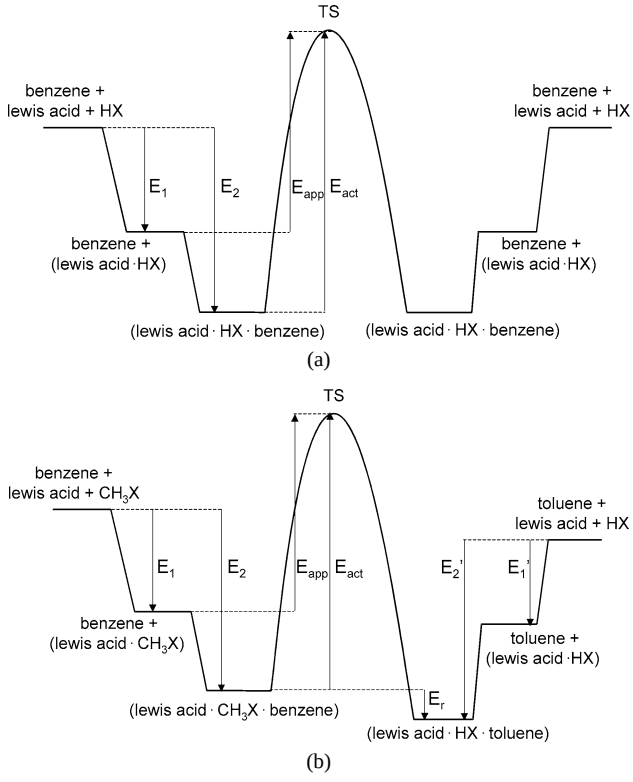

Fig. 3. Energy diagrams for the studied reactions (a) H-exchange of benzene, (b) methylation of benzene. The interaction energies (E_1, E_2, E'_1, E'_2), activation energies (E_{act}, E_{app}), and reaction energies (E_r), used in Table 2 are indicated here.

or methylation reaction, followed by the name of the catalyst.

3.2. Interaction between Lewis acids and HX or CH_3X

The geometries of the complexes formed by the Lewis acids and the proton or methyl-donating molecules are summarized in Table 1. The optimized structures are shown in Fig. 4. Isolated $Al(OH)_3$, BF_3, or $AlCl_3$ are planar, but in contact with a HX or CH_3X molecule the Lewis acid is slightly distorted (dihedral angle is between -3.18 and $-18.19°$) and the AlO-, BF-, or AlCl-bond distances are elongated. This can be derived from the increase of the mean MX distances in Table 1. The distance between the central metal ion and the ligand of HX or CH_3X ($d(MX_1)$) is always longer than the distance between the central metal ion and the original ligands. The same is true for the $Al(OH)_2O$ part of the L_1 site and its interaction with water or methanol: $Al(OH)_2O$ is planar, but when water or methanol adsorb the Lewis center is slightly distorted and the AlO distances are elongated.

The distances B–F(H) and B–F(CH_3) are too long to draw a bond. BF_3 forms weakly bonded van der Waals complexes with HF and CH_3F: the complexation energy (E_1 in Table 2) is very small and the B–F(H) and B–F(CH_3) distances ($d(MX_1)$ in Table 1) are much longer than the other B–F distances (mean $d(MX)$ in Table 1). Other studies on the BF_3–HF and BF_3–CH_3F complexes gave similar results. Phillips et al. [58] compared the structure of BF_3-HF obtained by high level ab initio calculations with the experimental structure obtained by microwave spectroscopy. At the MP4/d95v++(2df,2p) level of theory the BF distance ($d(MX_1)$) was 2.45 Å. Correction for the basis set superposition error yielded a BF distance in the range 2.45–2.55 Å. The complexation energy was -14 to -16 kJ mol^{-1}. Analysis of the rotational spectra yielded a BF distance of 2.544 Å in excellent agreement with theoretical results. Van der Veken and Sluyts [59] calculated the BF distance ($d(MX_1)$) of BF_3–CH_3F to be 2.3216 Å at a MP2/6-31+G** level. This is in close agreement with the distance of 2.42 Å obtained by microwave spectroscopy [60]. Van der Veken and Sluyts [59] also compared the calculated complexation energy of BF_3–CH_3F, which was -25.97 kJ mol^{-1}, with the experimental complexation energy. In liquid krypton this energy was -18.0 kJ mol^{-1}, but after correction for the solvent effect it increased to -23.4 kJ mol^{-1}, in good agreement with the calculated one. Both HF and CH_3F form weakly bonded van der Waals complexes with BF_3. In the gas phase no ion pairs (BF_4^- H^+ or BF_4^- CH_3^+) are formed.

Charge transfer between the Lewis acid and HX or CH_3X occurs: Lewis acids are electron acceptors and donation of electrons by HX or CH_3X to the Lewis acids creates a positive charge on HX or CH_3X.

Note that the $Al(OH)_3$–H_2O and the $Al(OH)_3$–CH_3OH complexes are similar to T_1-cluster models of a Brønsted acid site [61]. In the $Al(OH)_3$–H_2O complex Al is tetrahedrally coordinated and carries and OH group in the same way as the acid T_1 cluster, while $Al(OH)_3$–CH_3OH corresponds the a T_1 cluster with a methoxy group. Note also that mod-

Table 1
Geometry of isolated molecules and their interaction complexes (distances in Å, dihedral angle in degrees), charge separation q between Lewis acid, and interacting HX or CH_3X (in electron)

	Isolated molecules				Lewis acid–HX complex				Lewis acid–CH_3X complex			
	$Al(OH)_3$	BF_3	$AlCl_3$	L site	$Al(OH)_3$	BF_3	$AlCl_3$	L site	$Al(OH)_3$	BF_3	$AlCl_3$	L site
MX (mean)	1.708	1.321	2.087	1.704	1.737	1.324	2.106	1.732	1.738	1.326	2.115	1.734
$X_2X_3X_4M$	0.00	0.00	0.00	0.02	−14.10	−3.18	−14.10	−14.38	−16.95	−4.86	−18.19	−16.39
MX_1	–	–	–	–	1.988	2.552	2.634	1.981	1.967	2.383	2.477	1.965
HX_1	0.965	0.929	1.287	0.965	0.973	0.930	1.293	0.972	–	–	–	–
CX_1	1.426	1.399	1.806	1.426	–	–	–	–	1.450	1.413	1.831	1.450
q_{HX} or q_{CH_3X}	–	–	–	–	0.110	0.172	0.152	0.112	0.107	0.030	0.195	0.108

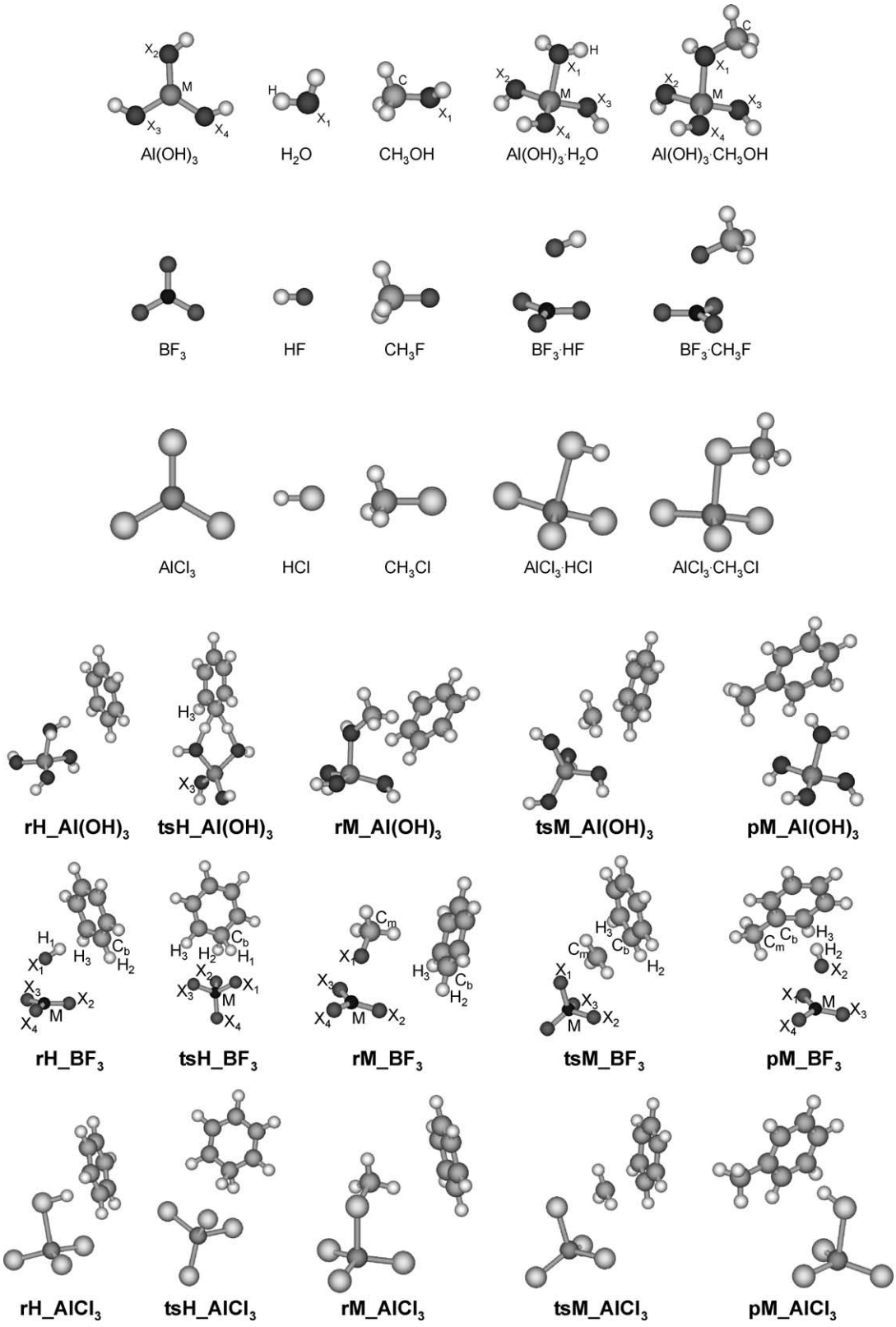

Fig. 4. Optimized structures: (a) All structures involved in the H-exchange and methylation of benzene catalyzed by gas-phase Lewis acids ($Al(OH)_3$, BF_3, and $AlCl_3$). (b) Interaction complexes of molecules with the L_1 site.

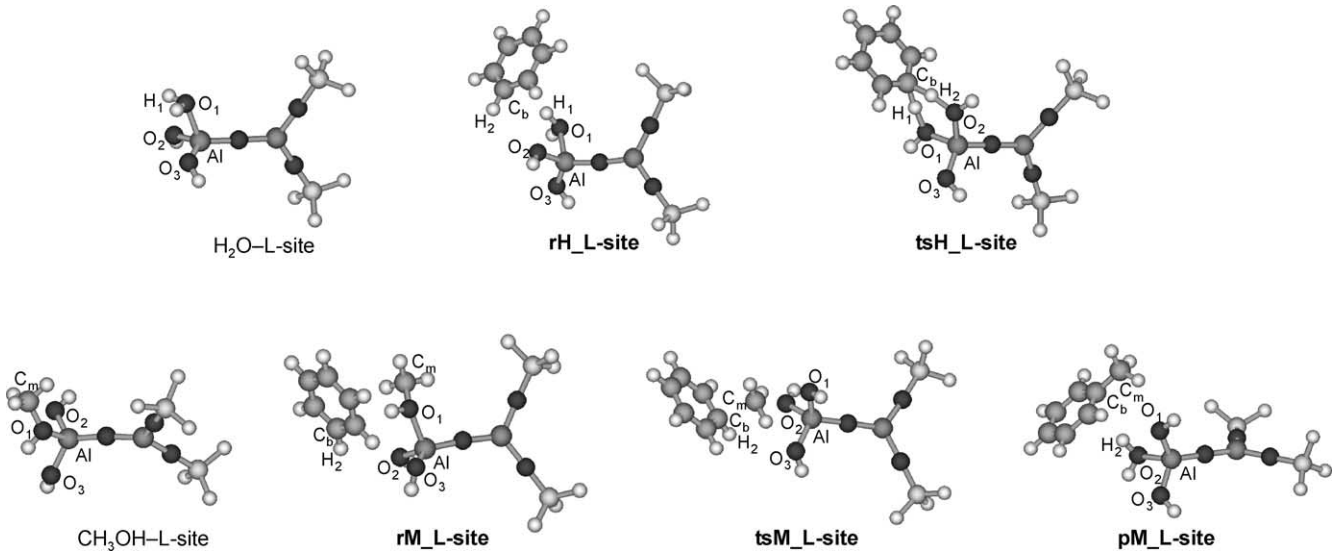

Fig. 4. Continued.

Table 2
Energy differences in kJ mol^{-1} (for definition, see Fig. 2), imaginary frequency at the transition structure (ν) in cm^{-1}, charge on benzenium ion at transition structure ($q_{C_6H_7}$) in e for H-exchange reactions, and charge on methyl group at transition structure (q_{CH_3}) in e for methylation reactions

	H-exchange				Methylation			
	$Al(OH)_3$	BF_3	$AlCl_3$	L_1 site	$Al(OH)_3$	BF_3	$AlCl_3$	L_1 site
E_1	−80.85	−8.21	−16.24	−82.50	−90.65	−11.94	−39.44	−91.48
E_2	−97.63	−24.91	−39.16	−99.47	−99.09	−15.17	−46.12	−106.34
E_{act}	115.22	95.67	33.91	114.49	214.46	136.61	96.54	216.06
E_{app}	98.44	78.97	10.99	15.01	206.01	133.39	89.87	109.72
E_r	0.00	0.00	0.00	0.00	−60.05	−63.51	−27.61	−55.52
E'_1	–	–	–	–	−80.85	−8.21	−16.24	−82.50
E'_2	–	–	–	–	−99.51	−26.86	−40.88	−102.24
ν	1362.55i	46.38i	14.44i	1345.58i	311.31i	311.97i	321.30i	285.97i
$q_{C_6H_7}/q_{CH_3}$	0.585	0.873	0.800	0.587	0.402	0.455	0.384	0.395

eling the Brønsted acid site of a zeolite as a Lewis acid in interaction with a proton-donating group is not so unrealistic, as the original model of the bridging hydroxyl group in zeolites is a Si–OH group in interaction with tri-coordinated Al [62].

3.3. Reaction mechanism for H-exchange of benzene

The H-exchange of benzene catalyzed by $Al(OH)_3$, BF_3, $AlCl_3$, or the L_1 site proceeds in one step, with an almost symmetrical transition structure (see Fig. 4 and Table 3). At the transition structure the proton of H_2O, HF, or HCl is attached to benzene and the charge on the Wheland-like C_6H_7 fragment is 0.55, 0.78, 0.71, and 0.54 e for, respectively, tsH_$Al(OH)_3$, tsH_BF_3, tsH_$AlCl_3$, and tsH_L site. The geometry of the isolated Wheland intermediate in the gas phase is given in Fig. 5c. Comparison shows that the distances between C_b and the proton are longer in tsH_$Al(OH)_3$, tsH_BF_3, tsH_$AlCl_3$, and tsH_L site than in the isolated Wheland intermediate and the $H_1C_bH_2$ angles are smaller. For tsH_BF_3 and tsH_$AlCl_3$, the C_6H_7 fragment is stabilized by close interaction between a nonexchanging proton of benzene (H_3) and a ligand of the Lewis acid (X_3). For tsH_$Al(OH)_3$ and tsH_L site this extra stabilization does not exist, but here the charge on the C_6H_7 fragment is smaller and the C_6H_7 fragment approaches the catalytic site closer.

The activation energies are 115.22, 95.67, 33.91, and 114.49 kJ mol^{-1} for $Al(OH)_3$, BF_3, $AlCl_3$, and the L_1 site, respectively (see Table 2). Hence, $AlCl_3$ is the most active catalyst as it reduces the activation energy most, followed by BF_3 and by the L_1 site and $Al(OH)_3$. The imaginary frequencies are very small for BF_3 and $AlCl_3$ (46.38i and 14.44i cm^{-1}). For $Al(OH)_3$ and the L_1 site the imaginary frequencies are higher (1362.55i and 1345.58i cm^{-1}. The magnitude of the imaginary frequency is an indication for the curvature of the potential energy surface (PES) at the transition structure: in the case of a BF_3 or a $AlCl_3$ catalyst the PES is more flat than for the two other catalysts.

This one-step reaction mechanism is in accordance with MP2/6-31+G** calculations by Heidrich [63] on the benzene–HF–BF_3 supermolecule, where an activation energy of 130.54 kJ mol^{-1} and similar geometries for the different stationary points were found.

Table 3
Geometry of interacting reactants, transition structures, interacting products for H-exchange, and methylation of benzene catalyzed by different Lewis acids (in Å)

	H-exchange		Methylation		
	Reactants	TS	Reactants	TS	Products
$Al(OH)_3$	$rH\_Al(OH)_3$	$tsH\_Al(OH)_3$	$rM\_Al(OH)_3$	$tsM\_Al(OH)_3$	$pM\_Al(OH)_3$
MX_1	1.936	1.834	1.955	1.819	1.749
X_1H_1/X_1C_m	0.979	1.352	1.450	2.449	3.564
H_1C_b/C_mC_b	2.228	1.293	3.897	1.942	1.511
C_bH_2	1.086	1.293	1.807	1.091	2.517
H_2X_2	2.838	1.352	2.369	2.628	0.980
X_2M	1.747	1.834	1.742	1.786	1.960
H_3X_3	4.283	4.043	4.289	3.620	4.418
$X_1H_1C_b/X_1C_mC_b$	171.07	173.55	151.97	151.97	88.83
$C_bH_2X_2$	114.67	173.55	132.50	132.50	163.68
BF_3	rH_BF_3	tsH_BF_3	rM_BF_3	tsM_BF_3	pM_BF_3
MX_1	2.384	1.445	2.362	1.472	1.331
X_1H_1/X_1C_m	0.942	1.776	1.417	2.209	3.823
H_1C_b/C_mC_b	2.287	1.138	4.031	2.009	1.510
C_bH_2	1.086	1.138	1.086	1.088	2.637
H_2X_2	3.151	1.776	3.122	4.028	0.945
X_2M	1.330	1.445	1.326	1.412	2.373
H_3X_3	4.312	2.290	4.766	4.552	6.215
$AlCl_3$	rH_AlCl_3	tsH_AlCl_3	rM_AlCl_3	tsM_AlCl_3	pM_AlCl_3
MX_1	2.503	2.207	2.459	2.245	2.114
X_1H_1/X_1C_m	1.326	2.231	1.837	2.608	5.256
H_1C_b/C_mC_b	2.116	1.136	3.925	2.067	1.510
C_bH_2	1.087	1.136	1.086	1.088	2.876
H_2X_2	3.376	2.229	3.582	4.017	1.328
X_2M	2.119	2.207	2.120	2.170	2.505
H_3X_3	3.501	2.767	6.242	4.478	3.417
L_1 site	rH_L site	tsH_L site	rM_L site	tsM_L site	pM_L site
MX_1	1.957	1.829	1.944	1.813	1.746
X_1H_1/X_1C_m	0.979	1.357	1.449	2.460	3.682
H_1C_b/C_mC_b	2.296	1.291	3.977	1.918	1.511
C_bH_2	1.086	1.292	1.087	1.090	2.496
H_2X_2	2.774	1.353	3.417	3.255	0.980
X_2M	1.744	1.831	1.744	1.784	1.954
H_3X_3	4.800	4.525	2.612	4.055	4.526

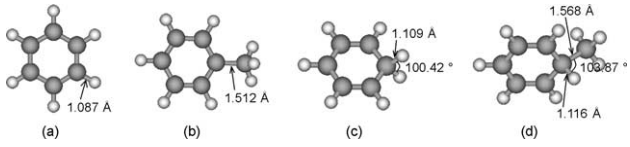

Fig. 5. B3LYP/6-31+G** optimized structures of isolated molecules, with some characteristic bond distances and bond angles: (a) benzene, (b) toluene, (c) protonated benzene, (d) protonated toluene.

3.4. Reaction mechanism for methylation of benzene

The geometries of reactants, transition structures, and products, all interacting with the Lewis acid catalysts, for methylation of benzene are given in Fig. 4 and Table 3. The reactions proceed in one step and at the transition structure the methyl group is somewhere in between X_1 and C_b. The methyl group is planar and resembles a methyl cation. The charge on the methyl is between 0.30 and 0.39 *e* at the transition structures. Because the methyl group is not yet attached to benzene, the transition structures do not resemble to a Wheland intermediate (see Fig. 5d).

The activation energies are 214.46, 136.61, 96.54, and 216.06 kJ mol^{-1} for $Al(OH)_3$, BF_3, $AlCl_3$, and the L_1 site, respectively (see Table 2). Hence, $AlCl_3$ is the most active catalyst as it reduces the activation energy most, followed by BF_3, $Al(OH)_3$, and the L_1 site The imaginary frequencies are between 286i and 322i cm^{-1}. For $rM\_Al(OH)_3$, tsM_AlCl_3, and pM_AlCl_3, the geometry was optimized with one additional very small imaginary frequency (18.75i, 8.83i, and 25.34i cm^{-1} for, respectively, $rM\_Al(OH)_3$, tsM_AlCl_3, and pM_AlCl_3). Our attempts to remove them failed.

3.5. Complete reaction path at the AM1 level

Understanding a reaction mechanism implies knowledge of the atomic rearrangements between the reactants and the

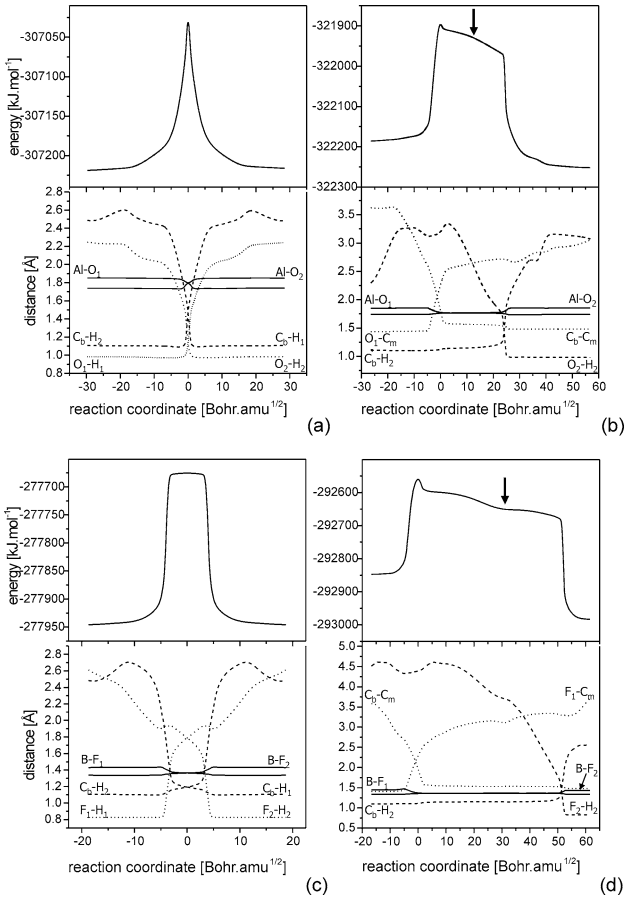

Fig. 6. Variation of energy and atomic distances during reaction: (a) H-exchange of benzene with HF catalyzed by BF_3, (b) methylation of benzene with CH_3F catalyzed by BF_3, (c) H-exchange of benzene with H_2O catalyzed by L_1 site, (d) methylation of benzene with CH_3OH catalyzed by L_1 site. The reaction coordinate is expressed in mass-weighted coordinates and the zero point of the reaction coordinate is situated at the transition structure. The arrows represent the points at which the geometries of (b) and (c) were taken.

transition structure and between the transition structure and the products. Starting from reoptimized transition structures at the AM1 level, intrinsic reaction coordinates (IRC) were reconstructed by following the steepest descent path toward reactants at one side and products at the other side. The AM1 level of calculation is the result of balancing the cost of IRC calculations and the quality of the obtained structures. For all reactions, the obtained geometries of reactants, transition structures, and products are similar to those calculated at the B3LYP/6-31+G** level and no additional reaction intermediates appeared. Therefore we concluded that the reaction mechanisms emerging from AM1 or B3LYP/6-31+G** are essentially the same. The IRCs allow monitoring of energy and atomic distances during reaction. In Fig. 6 some typical IRCs are shown. All reactions proceed in one step without formation of stable intermediates. The IRCs for the H-exchange of benzene are symmetrical, while the bond distances during methylation of benzene indicate that methylation of benzene occurs at the transition structure

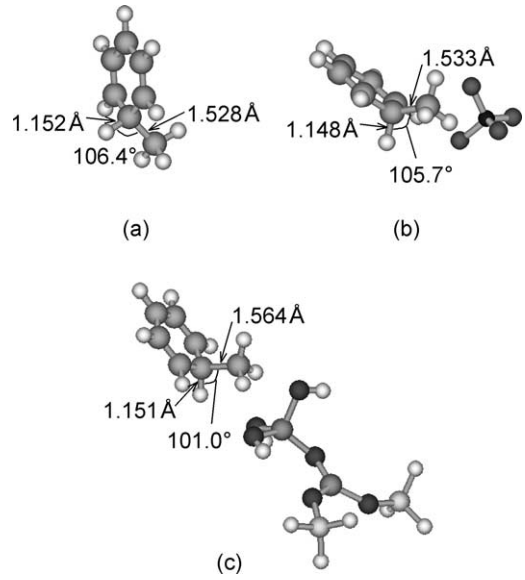

Fig. 7. AM1 results: (a) isolated Wheland intermediate in the gas phase, (b) Wheland-like structure for methylation of benzene catalyzed by BF_3, (c) Wheland-like structure for methylation of benzene catalyzed by L_1 site. (b) and (c) were obtained by calculation of the IRC (see Fig. 5).

and backdonation of a proton occurs a while after the transition structure. For the H-exchange reaction the transition structure corresponds to an ion pair, but for the methylation of benzene the transition structure does not correspond to an ion pair. Here the ion pair is in the process of being formed at the transition structure (reaction coordinate is zero Bohr amu$^{1/2}$) and is formed shortly after the transition structure. This ion pair (Figs. 7(b and c)) then has to rotate before it can give back a proton to the catalytic site (at, respectively, 50 and 25 Bohr amu$^{1/2}$ for BF_3 and the L_1 site as catalyst). The potential energy surface during rotation of the ion pair is very flat, but no local minimum is found and consequently no stable intermediate is formed.

3.6. General considerations about the reaction path

All studied reactions follow a concerted pathway with a cyclic transition structure. However a concerted reaction does not mean that all the bonds are broken or formed to the same extent at the transition structure [64]. For the H-exchange reactions, the H_1C_b bond is almost completely formed at the transition structure while the H_2C_b bond is far from being broken. For the methylation reactions the bond between the carbon atom of the methyl group (C_m) and the carbon atom of benzene (C_b) is in the process of being formed, while the breaking of the H_2C_b bond still has to occur.

This asynchronous pathway does not result in the formation of stable charged intermediates, while in the presence of a solvent Wheland intermediates are observed and the reactions proceed in two steps. These Wheland intermediates are ion pairs and are not stable in the gas phase. Although for some molecules stable ion pairs exist in the gas phase, e.g.,

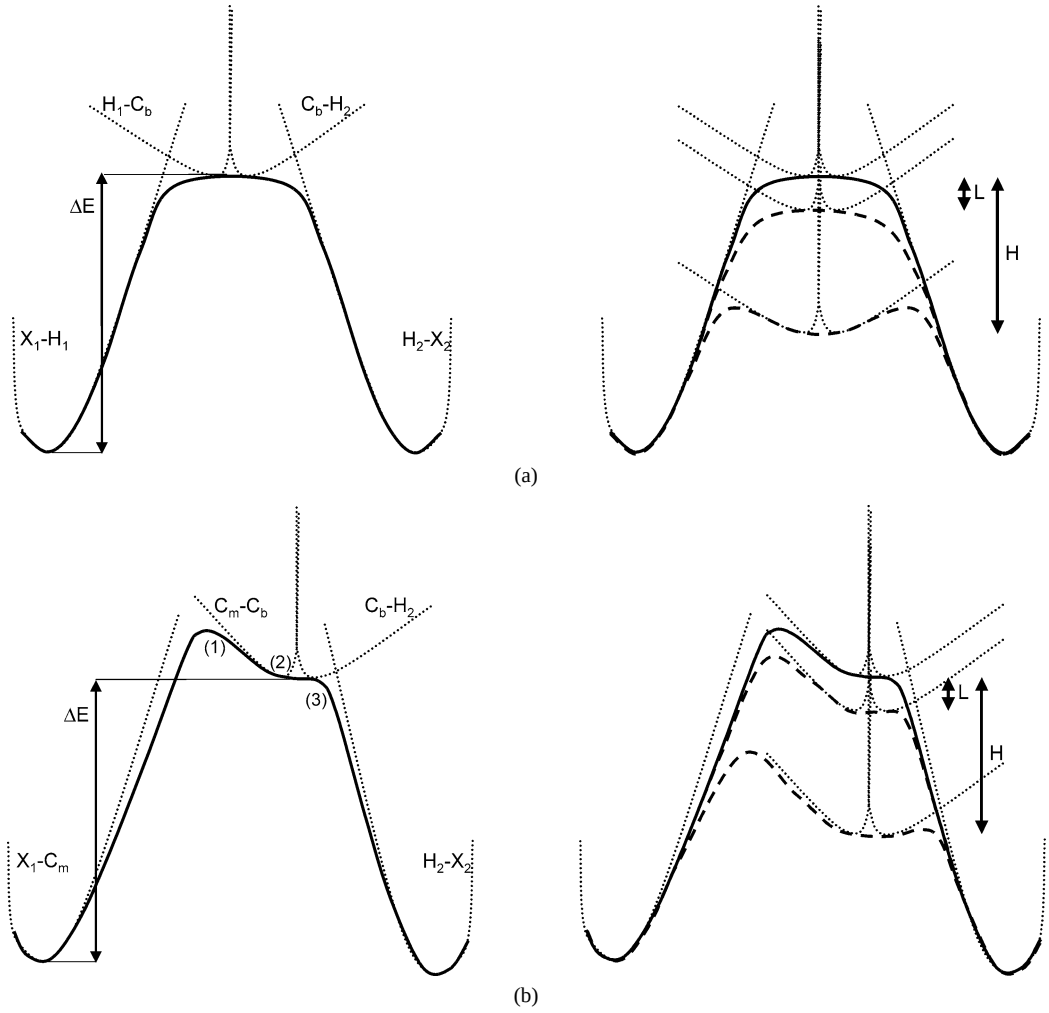

Fig. 8. Schematic picture of the reaction mechanisms of (a) H-exchange of benzene and (b) methylation of benzene. The solid line represents the reaction profile (IRC) as it is calculated in this study (gas-phase reactions). The dotted lines represent the potential energy curves of the bonds that are broken/formed during the reaction. These potential energy curves are responsible for the shape of the IRC. ΔE is the energy difference between the ion pair and the reactant molecule and the arrows L and H represent the stabilization of ion pair in a low (L) or high (H) polar environment. The more polar the environment, the more the ion pair will be stabilized (ΔE becomes smaller). The resulting reaction profiles in a polar environment are drawn in dashed lines. When the stabilization by the environment is large enough, not only the activation barrier will be lower but the ion pair can become a stable molecule, i.e., an intermediate.

NH_4^+–BF_4^-, NH_4^+–BCl_4^-, and H_3O^+–BCl_4^- [65], benzenium ion pairs are not stable. According to Heidrich [63] this can be explained by the fact that benzene is a large molecule where the charge is delocalized over the whole aromatic ring. When an ion pair is formed, not all the atoms carrying a positive charge can be stabilized by interaction with the counter ion. When the stabilization by solvent molecules covers a large volume, these ion pairs can become stable minima. An analogous effect was observed by Re et al. [66] for a HSO_4^- H_3O^+ ion pair, which becomes stable when the number of surrounding water molecules increases.

When the polarity of the transition structure is larger than that of the reactants, the transition structure is stabilized more by a polar environment and the activation energy of the reaction is lowered. In reactions catalyzed by enzymes this phenomenon is known as electrostatic catalysis [67,68].

For the reactions studied here a similar effect can be expected. Inside the cages and pores of a zeolite, electric field is present, making the environment for the molecules more polar [69–71]. The transition structure of the H-exchange is an ion pair and that of the methylation resembles closely an ion pair. These ion pairs are stabilized inside zeolites. The reactant molecules are less polar and are less stabilized, resulting in a lower activation energy for the reaction [72]. The more polar the environment, the more pronounced this effect will be.

We believe that when the electrostatic stabilization of the ion pairs is large enough—although this is not necessary the case inside zeolites, but possibly in a suitable solvent—not only the activation barrier is lowered but also the reaction mechanism can change from a one-step reaction to a two-step reaction with formation of a stable intermediate. In Fig. 8 the IRCs for H-exchange and methylation of benzene are drawn schematically (full lines). The shape of these IRCs is the result of the superposition of potential energy curves of the bonds broken or formed in the reaction (dot-

ted lines) [73–75]. The dashed lines represent hypothetical reaction mechanisms in a polar solvent. In what follows the effect of the environment on the shape of the reaction profile will be discussed in detail for the H-exchange and for the methylation reaction.

For the H-exchange reaction the transition structure corresponds to an ion pair, with a charge separation between 0.587 and 0.873 *e* (Table 2). The potential energy surface, PES, around this ion pair is flat as can be deduced from the low imaginary frequency of the transition structures (Table 2). When the electrostatic stabilization of a solvent becomes large enough, the relative energy differences of the individual energy curves can change enough to make the ion pair a local minimum. Between two local minima there is always a transition structure: between reactants and the intermediate there is one transition structure and also between the intermediate and the products. The reaction now follows a two-step mechanism. In the first step the proton is attached to benzene to form a Wheland intermediate, in the second step a proton is expelled.

For the methylation of benzene, the transition structure does not correspond to an ion pair. According to the AM1 calculations of the IRC, the ion pair is in the process of being formed at the transition structure and is formed shortly after the transition structure ((1) in Fig. 8). This ion pair then has to rotate ((2) in Fig. 8 and Figs. 7b and c) before it can give back a proton to the catalyst complex ((3) in Fig. 8). The PES during rotation of the ion pair is very flat. The electrostatic stabilization of a solvent can change the relative energy differences of the individual energy curves, making the ion pair a local minimum. As a consequence the reaction now follows a two-step mechanism with two transition structures: one for the attack of the methyl group on benzene and a second for the backdonation of a proton to the cluster. Between these two transition structures there is a local minimum corresponding to a stable Wheland intermediate.

Other theoretical calculations on the H-exchange and methylation of benzene catalyzed by the bridging hydroxyl groups or Brønsted acid sites of zeolites [24,61,76,77] all indicate that the reaction mechanism for these reactions is also concerted without formation of stable charged intermediates. Corma et al. [77] explored the PES for the methylation of benzene catalyzed by a Brønsted acid site of a zeolite using PM3. Because of the flatness of the PES, they proposed the existence of a Wheland intermediate. However, they could not find a second transition structure after this would be intermediate.

According to theoretical calculations the electrostatic potential generated by a zeolite lattice is not strong enough to turn ion pairs into local minima [78] and experimentally only the most stable carbocations can be observed [79–81]. When a solvent is used for zeolite-catalyzed reactions, only very few solvent molecules can surround the molecules or complexes at the active site inside the zeolite pores. The stabilization by the solvent will be much smaller than the stabilization in a pure solvent. Therefore, the existence of carbocations as reaction intermediates in zeolite-catalyzed reactions is unlikely.

We would like to end this discussion about the influence of the environment on the reaction path by stating that the influence of a liquid solvent on the reaction mechanism of zeolite-catalyzed reactions does not necessary lead to an increase in reaction rate. A polar solvent can indeed compete with the reactant molecules for adsorption on the active sites inside zeolites thus limiting the reaction rate [82].

4. Activity of the different catalysts

4.1. Reaction rate constants

The results of the kinetic analysis for the H-exchange and the methylation of benzene are given in Table 4 and Fig. 9. Reaction rate constants were calculated for the reactions starting from the isolated Lewis acids, HX, and CH_3X in the gas phase. However, because there exists a strong interaction

Table 4
Kinetic analysis of the studied reactions: k_r ($m^6\,s^{-1}\,mol^{-2}$ when starting for isolated molecules and $m^3\,s^{-1}\,mol^{-1}$ when starting from complexes), E_{Arr} ($kJ\,mol^{-1}$), A ($m^6\,s^{-1}\,mol^{-2}$ or $m^3\,s^{-1}\,mol^{-1}$), ΔS_{act} ($kJ\,mol^{-1}\,K^{-1}$), and ΔG_{act} ($kJ\,mol^{-1}$)

	H-exchange				Methylation			
	$Al(OH)_3$	BF_3	$AlCl_3$	L_1 site	$Al(OH)_3$	BF_3	$AlCl_3$	L_1 site
Starting from isolated Lewis acid and HX or CH_3X								
k_r (400 K)	8.08×10^{-9}	1.22×10^{-14}	1.05×10^{-5}	1.48×10^{-8}	2.21×10^{-21}	9.58×10^{-23}	1.61×10^{-17}	2.87×10^{-30}
E_{Arr}	26.23	78.27	5.78	25.13	131.80	137.40	65.14	193.61
A	2.75×10^{-5}	2.50×10^{-5}	7.43×10^{-5}	3.62×10^{-5}	4.94×10^{-4}	1.15×10^{-4}	6.70×10^{-6}	7.57×10^{-5}
ΔS_{act}	−0.262	−0.263	−0.254	−0.260	−0.238	−0.250	−0.275	−0.254
ΔG_{act}	124.54	176.89	100.78	122.51	220.50	230.94	168.14	288.55
Starting from Lewis acid–HX or Lewis acid–CH_3X complexes								
k_r (400 K)	6.57×10^{-11}	2.43×10^{-10}	$1.42\times10^{+1}$	1.62×10^{-10}	3.13×10^{-24}	2.10×10^{-17}	8.26×10^{-11}	6.15×10^{-32}
E_{Arr}	105.65	80.07	16.26	104.61	217.60	140.05	96.34	282.47
A	$4.72\times10^{+3}$	$7.59\times10^{+0}$	$2.09\times10^{+2}$	$8.50\times10^{+3}$	$9.86\times10^{+4}$	$4.82\times10^{+1}$	$3.52\times10^{+2}$	$6.00\times10^{+5}$
ΔS_{act}	−0.096	−0.150	−0.122	−0.092	−0.071	−0.135	−0.118	−0.056
ΔG_{act}	140.89	136.70	61.87	138.89	242.74	190.54	140.21	301.60

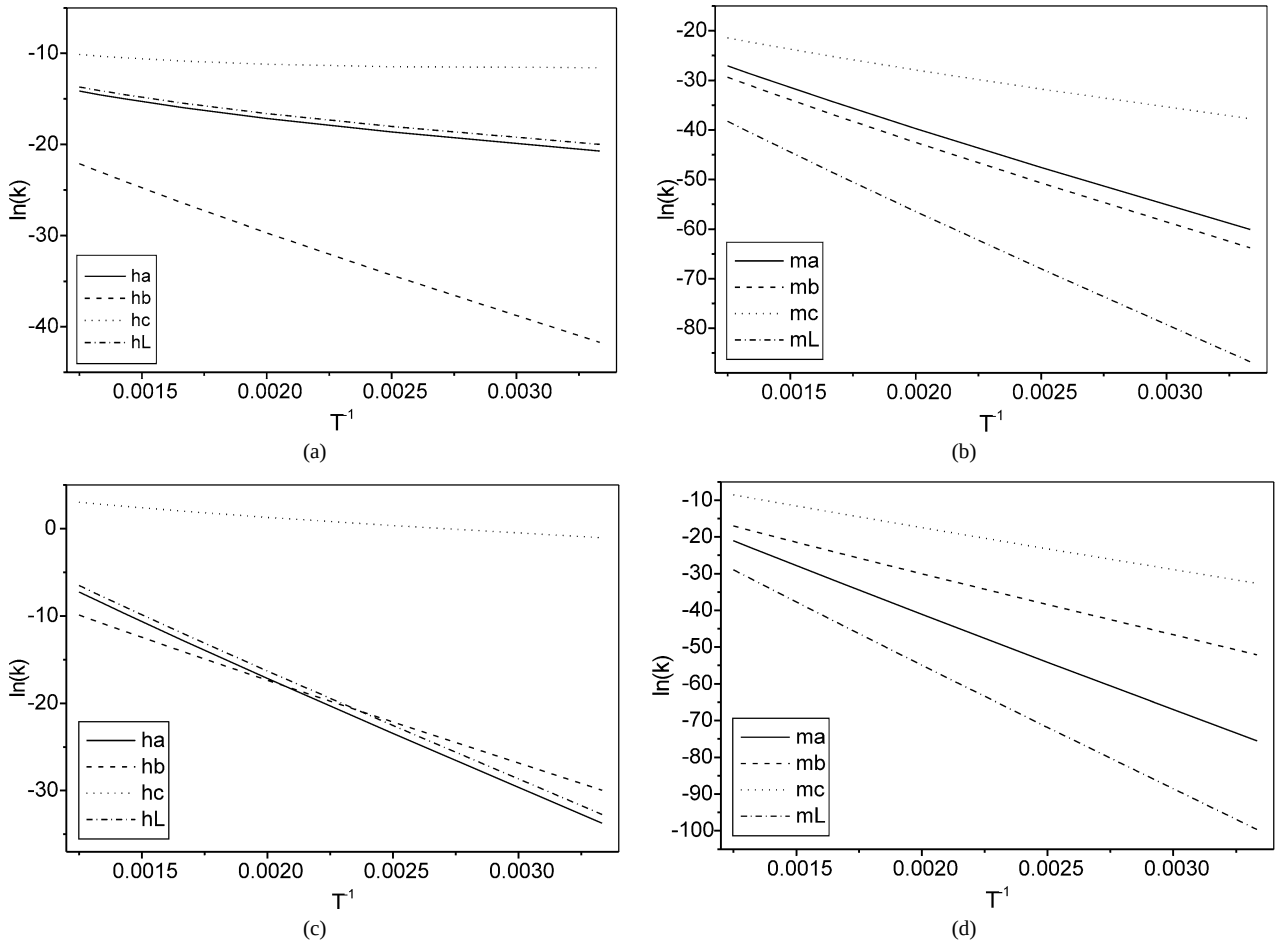

Fig. 9. Arrhenius plots (a) H-exchange starting from isolated Lewis acid an HX, (b) methylation starting for isolated Lewis acid and CH_3X, (c) H-exchange starting for Lewis acid–HX complexes, (d) methylation starting from Lewis acid–CH_3X complexes.

between the Lewis acid and the HX or CH_3X molecule, reaction rate constants were also calculated for reactions starting from a MX_3–HX or a MX_3–CH_3X complex.

In all cases $AlCl_3$ is the best catalyst in that it gives the highest rates. The differences in theoretical rate constants at 400 K cover a range of 10^6–10^{13}. The extreme cases are the H-exchange starting from isolated molecules and methylation starting from the complexes. These differences in rate constants can be largely ascribed to the activation energies, which are smallest for $AlCl_3$ in all cases studied.

The negative ΔS_{act} values indicate a decrease in entropy when going from reactants to transition state due to the loss of rotational and translational degrees of freedom. The values for ΔS_{act} differ much less than the values for k_r, but they are more negative for reactions starting from isolated molecules than for reactions starting from complexes. Reactions that start from the complexes are entropically favored because here all the reactant molecules are already close together while for reactions that start from isolated molecules, three different molecules have to collate.

A comparison of all the rate constants is summarized in Scheme 1. The efficiency of $AlCl_3$ as a catalyst is always higher than that of BF_3, in agreement with experimental studies on the relative efficiencies of metal halides in the alkylation of benzene [73,74]. For the H-exchange, $Al(OH)_3$ and the L_1 site of zeolites have comparable efficiency while for the methylation $Al(OH)_3$ is more efficient than the L_1 site. They both have a similar active center but the surrounding atoms, present in the L_1 site, seem to disfavor the reaction rate for the methylation of benzene. To calculate the influence of a complete zeolite lattice, crystal calculations seem to be necessary.

H-exchange	
• starting from isolated Lewis acid and HX	$AlCl_3$ > L-site ≈ $Al(OH)_3$ > BF_3
• starting from adsorption complexes	
below 420 K	$AlCl_3$ > BF_3 > L-site ≈ $Al(OH)_3$
above 480 K	$AlCl_3$ > L-site ≈ $Al(OH)_3$ > BF_3
Methylation	
• starting from isolated Lewis acid and CH_3X	$AlCl_3$ > $Al(OH)_3$ > BF_3 > L-site
• starting from adsorption complexes	$AlCl_3$ > BF_3 > $Al(OH)_3$ > L-site

Scheme 1. Reactivity sequence of the Lewis acids $Al(OH)_3$, BF_3, and $AlCl_3$ and the Lewis acid site of zeolites in the H-exchange and methylation of benzene, based on the reaction rate constants.

4.2. DFT-based reactivity descriptors

Global reactivity descriptors like the global hardness and activation hardness (Table 5) as well as local reactivity de-

Table 5
Global reactivity descriptors in atomic units for the studied reactions

	$\eta_{\text{reactants}}$	η_{TS}	η_{products}	$\Delta\eta_{\text{act}}$
		$\eta = (IE - EA)/2$		
H_Al(OH)$_3$	0.1685	0.1654	–	0.0031
H_BF$_3$	0.1798	0.1557	–	0.0241
H_AlCl$_3$	0.1781	0.1215	–	0.0566
H_L site	0.1651	0.1583	–	0.0061
M_Al(OH)$_3$	0.1624	0.1197	0.1636	0.0427
M_BF$_3$	0.1716	0.1492	0.1708	0.0223
M_AlCl$_3$	0.1715	0.1253	0.1721	0.0462
M_L site	0.1635	0.1151	0.1611	0.0483
		$\eta = (E_{\text{HOMO}} - E_{\text{LUMO}})/2$		
H_Al(OH)$_3$	0.1199	0.1010	–	0.0188
H_BF$_3$	0.1204	0.0838	–	0.0366
H_AlCl$_3$	0.1160	0.0534	–	0.0626
H_L site	0.1171	0.1030	–	0.0141
M_Al(OH)$_3$	0.1155	0.0519	0.1149	0.0636
M_BF$_3$	0.1210	0.0794	0.1141	0.0417
M_AlCl$_3$	0.1112	0.0602	0.1134	0.0511
M_L site	0.1172	0.0541	0.1114	0.0632

scriptors like the differences between atomic softnesses or atomic hardnesses of interacting atoms (Table 6) have been calculated in order to compare the activity of the different catalysts.

The global hardnesses of the different structures are given in Table 5. The hardness of the transition structure is smaller than the hardness of interacting reactants or products. This is in agreement with the maximum hardness principle [34]: Molecules arrange themselves so as to be as hard as possible. Therefore stable structures with low energy (here reactants and products) are likely to be harder than less stable structures with high energy (here transition structures).

The activation hardness, $\Delta\eta_{\text{act}} = \eta_{\text{reactants}} - \eta_{\text{TS}}$ was introduced by Zhou and Parr [85] for describing the selectivity of electrophilic aromatic substitutions. In reactions for which the starting points, i.e., interacting reactants are similar, $\Delta\eta_{\text{act}}$ correlates with the activation energy. Here $\Delta\eta_{\text{act}}$ does not correlate with E_{act} meaning that $\Delta\eta_{\text{act}}$ is less suited to explain reactivity sequences for reactions with different reactant molecules and we were not able to generalize the concept of activation hardness.

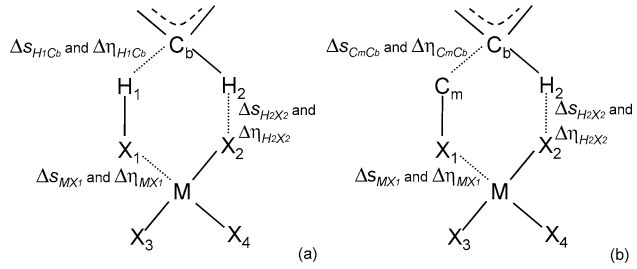

Fig. 10. Δs_{AB} and $\Delta\eta_{\text{AB}}$ used in Table 6 for (a) H-exchange of benzene, (b) methylation of benzene.

The local reactivity descriptors, which are used in the local HSAB principle, are given in Table 6. For each reaction, six different local reactivity descriptors are calculated [Eqs. (7)–(11)] and the symbols are explained in Fig. 10. The atomic interactions between reactants and catalyst are of an electrophilic–nucleophilic nature. There are three important pairs of such electrophilic–nucleophilic interacting atoms: (1) M–X_1, (2) H_1–C_b or C_m–C_b, and (3) H_2–X_2. These atomic interactions are partly orbital controlled and partly charge controlled, and therefore both Δs_{AB} and $\Delta\eta_{\text{AB}}$ are calculated for all three atomic interaction pairs. In multicenter interaction complexes like the structures investigated here, none of the calculated local reactivity descriptors on its own can take into account all the interactions that are important. Therefore, following the approach of Pal and coworkers [57] and the present authors [43], a sum of squares of the Δs_{AB} values was calculated. By analogy also the sum of squares of the $\Delta\eta_{\text{AB}}$ values was calculated.

The $\Sigma(\Delta s_{\text{AB}})^2$ values should be as small as possible to promote the reaction. In Table 6 we can see that for both the H-exchange and methylation of benzene, $AlCl_3$ as a catalyst has a lower value than BF_3. This is in agreement with the calculated reaction rate constants and with experimental results [83,84], demonstrating that $AlCl_3$ is a better catalyst than BF_3. The $\Sigma(\Delta s_{\text{AB}})^2$ values of Al(OH)$_3$ and the L_1 site differ a lot, the value of the L_1 site being much smaller than the value of Al(OH)$_3$. This means that the L_1 site is expected to be more active than Al(OH)$_3$. However, we were not able to see the same activity sequence in the calculated reaction rate constants (Fig. 9 and Table 4). So we have a problem for discriminating between Al(OH)$_3$ and the L_1 site, which have chemically similar active centers consisting of $(HO)_2$–

Table 6
Local reactivity descriptors in atomic units for the studied reactions

	H-exchange					Methylation			
	Al(OH)$_3$	BF$_3$	AlCl$_3$	L_1 site		Al(OH)$_3$	BF$_3$	AlCl$_3$	L_1 site
Δs_{MX1}	1.2326	0.8256	0.3310	0.5266	Δs_{MX1}	1.3483	1.1193	0.1709	0.2515
Δs_{H1Cb}	1.1026	0.1464	0.2446	0.1474	Δs_{CmCb}	0.3513	0.6521	0.0511	0.2807
Δs_{H2X2}	0.2539	0.0678	0.2596	0.1635	Δs_{H2X2}	0.1948	0.0517	0.1800	0.2137
$\Sigma(\Delta s_{\text{AB}})^2$	1.5944	0.7077	0.2368	0.3257	$\Sigma(\Delta s_{\text{AB}})^2$	1.9794	1.6807	0.0643	0.1878
$\Delta\eta_{\text{MX1}}$	1.0570	0.9231	1.1628	1.1008	$\Delta\eta_{\text{MX1}}$	1.2451	1.1041	1.3297	1.2846
$\Delta\eta_{\text{H1Cb}}$	0.2633	0.3173	0.0060	0.2740	$\Delta\eta_{\text{CmCb}}$	0.0737	0.0372	0.3892	0.0739
$\Delta\eta_{\text{H2X2}}$	0.9800	0.2570	0.2428	0.9762	$\Delta\eta_{\text{H2X2}}$	0.9664	0.2594	0.2607	0.9750
$\Sigma(\Delta\eta_{\text{AB}})^2$	2.1471	1.0188	1.4110	2.2397	$\Sigma(\Delta\eta_{\text{AB}})^2$	2.4895	1.2876	1.9875	2.6063

Al–O–. According to one reactivity descriptor the L_1 site is more active than $Al(OH)_3$ for both the H-exchange and methylation reaction and according to the kinetic parameters both catalyst have more or less the same activity for the H-exchange but $Al(OH)_3$ is more active for the methylation. To the best of our knowledge there are no experimental studies available, which can shed some light on this issue.

In the reactions studied here, vacant orbitals of the Lewis acid catalysts interact with nonbonded electron pairs of the reactant molecules, resulting in reactions that are more orbital controlled and less charge controlled. This makes the local softness better suited than the local hardness for describing the intermolecular reactivity sequences of the reactions catalyzed by Lewis acids. It is therefore not surprising that $\Sigma(\Delta\eta_{AB})^2$ does not yield a good reactivity sequence.

5. Conclusion

Through density functional calculations on the optimized structures involved in the H-exchange and methylation of benzene catalyzed by various Lewis acid catalysts, these reactions can be better understood.

The reaction mechanisms of all the studied reactions are very similar in that the reactions are concerted and no stable charged intermediates are formed. This concerted mechanism does not mean that all the bonds are broken or formed synchronously. Some reflections about the influence of a solvent on this asynchronous one-step mechanism were made. For reactions carried out in the gas phase or inside a zeolite, ion pairs are not stable but in the presence of a suitable solvent these ion pairs can become local minima or stable intermediates and the reaction mechanism changes into a two-step mechanism.

On the basis of the calculated properties we are able to compare the activity of the different Lewis acids. $AlCl_3$ is always more active than BF_3, in agreement with experimental results. The ranking of $Al(OH)_3$ and the L_1 site of zeolites, which have comparable active centers, in this activity sequence is less obvious. According to the calculated $\Sigma(\Delta s_{AB})^2$ values the L_1 site is more active than $Al(OH)_3$, but no unambiguous trend could be extracted from the calculated reaction rate constants. Since also from experimental research neither the structure nor the acid strength of Lewis acid sites inside zeolites are understood, further research in this field is mandatory.

In contrast to reactivity descriptors based on the local hardness, the $\Sigma(\Delta s_{AB})^2$ values appear to be good reactivity descriptors for describing the intermolecular reactivity sequences of the reactions catalyzed by different Lewis acids.

Acknowledgments

This work has been performed with support from the G.O.A. (Geconcerteerde Onderzoeksactie Vlaanderen). The authors acknowledge the Free University of Brussels (V.U.B.) for a generous computer grant. A.M.V. is a postdoctoral fellow of the Fund for Scientific Research–Flanders (Belgium) (F.W.O.–Vlaanderen) and also thanks the I.W.T. for financial support. P.G. thanks the F.W.O.–Vlaanderen for continuous support of his group.

References

[1] R.T. Morrison, R.N. Boyd, Organic Chemistry, Prentice Hall, Englewood Cliffs, NJ, 1992.
[2] K. Weisselmel, H. Arpe, Industrial Organic Chemistry, Chemie, Weinheim, NY, 1994.
[3] J. Martens, W. Souverijns, W. Van Rhijn, P. Jacobs, in: G. Ertl, H. Knözinger, J. Weitkamp (Eds.), Handbook of Heterogeneous Catalysis, Wiley–VCH, Weinheim, 1997.
[4] F. Collignon, P.A. Jacobs, P. Grobet, G. Poncelet, J. Phys. Chem. B 105 (2001) 6812.
[5] A.I. Biaglow, D.J. Parrillo, G.T. Kokotailo, R.J. Gorte, J. Catal. 148 (1994) 213.
[6] J.R. Sohn, S.J. DeCanio, P.O. Fritz, J.H. Lunsford, J. Phys. Chem. 90 (1986) 4847.
[7] B. Schoofs, J.A. Martens, P.A. Jacobs, R.A. Schoonheydt, J. Catal. 183 (1999) 355.
[8] J. Sauer, Chem. Rev. 89 (1989) 199.
[9] G.J. Kramer, R.A. van Santen, C.A. Emeïs, A.K. Nowak, Nature 363 (1993) 529.
[10] R.A. van Santen, G.J. Kramer, Chem. Rev. 95 (1995) 37.
[11] S.R. Blaszkowski, R.A. van Santen, J. Am. Chem. Soc. 119 (1997) 5020.
[12] E. Sandré, M.C. Payne, J.D. Gale, Chem. Commun. (1998) 2445.
[13] I. Stich, J.D. Gale, K. Terakura, M.C. Payne, J. Am. Chem. Soc. 121 (1999) 3292.
[14] A.G. Pelmenschikov, R.A. van Santen, J. Janchen, E. Meijer, J. Phys. Chem. 97 (1993) 11071.
[15] S. Bates, J. Dwyer, J. Phys. Chem. 97 (1993) 5897.
[16] K.M. Neyman, V.A. Nasluzov, G.M. Zhidomirov, Catal. Lett. 40 (1996) 183.
[17] L. Benco, T. Demuth, J. Hafner, F. Hutschka, H. Toulhoat, J. Catal. 209 (2002) 480.
[18] A.A. Lamberov, A.M. Kuznetsov, M.S. Shapnik, A.N. Masliy, S.V. Borisevich, R.G. Romanova, S.R. Egorova, J. Mol. Catal. A 158 (2000) 481.
[19] M.J. Frisch, G.W. Trucks, H.B. Schlegel, M.A. Scuseria, M.A. Robb, J.R. Cheeseman, V.G. Zakrzewski, J.A. Montgomery, R.E. Stratmann, J.C. Burant, S. Dapprich, J.M. Millam, A.D. Daniels, K.N. Kudin, M.C. Strain, O. Farkas, J. Tomasi, V. Barone, M. Cossi, R. Cammi, B. Mennucci, C. Pomelli, C. Adamo, S. Clifford, J. Ochterski, G.A. Petersson, P.Y. Ayala, Q. Cui, K. Morokuma, D.K. Malick, D.K. Rabuck, K. Raghavachari, J.B. Foresman, J. Cioslowski, J.V. Ortiz, B.B. Stefanov, G. Liu, A. Liashenko, P. Piskorz, I. Komaromi, R. Gomperts, R.L. Martin, D.J. Fox, T. Keith, M.A. Al-Laham, C.Y. Peng, A. Nanayakkara, C. Gonzales, M. Challacombe, P.M.W. Gill, B.G. Johnson, W. Chen, M.W. Wong, J.L. Andress, M. Head-Gordon, E.S. Replogle, J.A. Pople, Gaussian 98 (revision A.7), Gaussian, Inc., Pittsburg, PA, 1998.
[20] A.D. Becke, J. Chem. Phys. 98 (1993) 5648.
[21] C. Lee, W. Yang, R.G. Parr, Phys. Rev. B 37 (1988) 785.
[22] A.H. Otto, Phys. Chem. Commun. (1999) 12.
[23] A.M. Vos, F. De Proft, R.A. Schoonheydt, P. Geerlings, Chem. Commun. (2001) 1108.
[24] A.M. Vos, K.H.L. Nulens, F. De Proft, R.A. Schoonheydt, P. Geerlings, J. Phys. Chem. B 106 (2002) 2026.
[25] A.M. Vos, R.A. Schoonheydt, F. De Proft, P. Geerlings, J. Phys. Chem. B 107 (2003) 2001.

[26] M.J.S. Dewar, E.G. Zoebisch, E.F. Healy, J.J.P. Stewart, J. Am. Chem. Soc. 107 (1985) 3902.
[27] M.W. Schmidt, K.K. Baldridge, J.A. Boatz, S.T. Elbert, M.S. Gordon, J.H. Jensen, S. Koseki, N. Matsunaga, K.A. Nguyen, S.J. Su, T.L. Windus, M. Dupuis, J.A. Montgomery, J. Comput. Chem. 14 (1993) 1347.
[28] C. Gonzalez, H.B. Schlegel, J. Phys. Chem. 94 (1990) 5523.
[29] C. Gonzalez, H.B. Schlegel, J. Chem. Phys. 95 (1991) 5853.
[30] H. Eyring, J. Chem. Phys. 3 (1934) 107.
[31] S. Glasstone, Physical Chemistry, Van Nostrand, Toronto, 1946.
[32] P.J. Robinson, J. Chem. Educ. 55 (1978) 509.
[33] A.P. Scott, L. Radom, J. Phys. Chem. 100 (1996) 16502.
[34] R.G. Pearson, Chemical Hardness, Wiley–VCH, Weinheim, 1997.
[35] R.G. Parr, W. Yang, Density Functional Theory of Atoms and Molecules, Oxford Univ. Press, Oxford, 1989.
[36] R.G. Parr, W. Yang, Annu. Rev. Phys. Chem. 46 (1995) 701.
[37] P. Geerlings, F. De Proft, W. Langenaeker, Adv. Quant. Chem. 39 (1999) 303.
[38] H. Chermette, J. Comp. Chem. 20 (1999) 129.
[39] F. De Proft, P. Geerlings, Chem. Rev. 101 (2001) 1451.
[40] P. Geerlings, F. De Proft, W. Langenaeker, Chem. Rev. 103 (2003) 1793.
[41] R.G. Pearson, R.G. Parr, J. Am. Chem. Soc. 105 (1983) 7512.
[42] J.L. Gazquez, F. Mendez, J. Phys. Chem. 98 (1994) 4591.
[43] S. Damoun, G. Van de Woude, S. Mendez, P. Geerlings, J. Phys. Chem. A 101 (1997) 886.
[44] P. Geerlings, F. De Proft, Int. J. Quant. Chem. 80 (2000) 227.
[45] F. De Proft, R. Vivas-Reyes, M. Biesemans, R. Willem, J.M.L. Martin, P. Geerlings, Eur. J. Inorg. Chem., in press.
[46] W. Yang, R.G. Parr, Proc. Natl. Acad. Sci. USA 82 (1985) 6723.
[47] R.G. Parr, W. Yang, J. Am. Chem. Soc. 106 (1984) 4049.
[48] K. Fukui, T. Yonezawa, H. Shingu, J. Chem. Phys. 20 (1952) 722.
[49] W. Yang, W.J. Mortier, J. Am. Chem. Soc. 108 (1986) 5708.
[50] A.E. Reed, R.B. Weinstock, F. Weinhold, J. Chem. Phys. 83 (1985) 735.
[51] M. Berkowitz, R.G. Parr, J. Chem. Phys. 88 (1988) 2554.
[52] M.K. Harbola, P.K. Chattaraj, R.G. Parr, Isr. J. Chem. 31 (1991) 395.
[53] M. Berkowitz, S.K. Ghosh, R.G. Parr, J. Am. Chem. Soc. 107 (1985) 6811.
[54] W. Langenaeker, F. De Proft, P. Geerlings, J. Phys. Chem. 99 (1995) 6424.
[55] P. Geerlings, W. Langenaeker, F. De Proft, A. Baeten, Molecular Electrostatic Potentials—Concepts and Applications, in: Theoretical and Computational Chemistry, Vol. 3, 1996, p. 587.
[56] P.K. Chattaraj, J. Phys. Chem. A 105 (2001) 511.
[57] K.R.S. Chandrakumar, S. Pal, J. Phys. Chem. A 106 (2002) 5737.
[58] J.A. Phillips, M. Canagaratna, H. Goodfriend, A. Grushow, J. Almlöf, K.R. Leopold, J. Am. Chem. Soc. 117 (1995) 12549.
[59] B.J. van der Veken, E.J. Sluyts, J. Phys. Chem. A 101 (1997) 9070.
[60] K.R. Leopold, M. Canagaratna, J.A. Phillips, Acc. Chem. Res. 30 (1997) 57.
[61] S.R. Blaszkowsi, R.A. van Santen, in: D.G. Thuhlar, K. Morokuma (Eds.), Transition State Modeling for Catalysis, in: ACS Symp. Ser., Vol. 721, 1999, p. 307.
[62] J.B. Uytterhoeven, L.G. Christner, W.K. Hall, J. Phys. Chem. 69 (1965) 2117.
[63] D. Heidrich, Phys. Chem. Chem. Phys. 1 (1999) 2209.
[64] T.L. Gilchrist, R.C. Storr, Organic Reactions and Orbital Symmetry, Cambridge Univ. Press, Cambridge, UK, 1978.
[65] N.J.R. van Eikema Hommes, D. Heidrich, P. von Ragué Schleyer, J. Mol. Model. 6 (2000) 563.
[66] S. Re, Y. Osamura, K. Morokuma, J. Phys. Chem. A 103 (1999) 3535.
[67] G. Naray-Szabo, J. Mol. Struct. (Theochem.) 500 (2000) 157.
[68] P.B. Rupert, A.P. Massey, S.T. Sigurdsson, A.R. Ferré-D'amaré, Science 298 (2002) 1421.
[69] G.O.A. Janssens, B.G. Baekelant, H. Toufar, W.J. Mortier, R.A. Schoonheydt, J. Phys. Chem. 99 (1995) 3251.
[70] R.C. Deka, R. Vetrivel, Chem. Commun. (1996) 3297.
[71] R.C. Deka, R. Vetrivel, J. Catal. 174 (1998) 88.
[72] X. Rozanska, R.A. van Santen, F. Hutschka, J. Hafner, J. Catal. 215 (2003) 20.
[73] J. Horiuti, M. Polanyi, J. Mol. Catal. A 199 (2003) 185.
[74] J. Stevens, M. Schweizer, G. Rauhut, J. Am. Chem. Soc. 123 (2001) 7326.
[75] G. Rauhut, Phys. Chem. Chem. Phys. 5 (2003) 791.
[76] L.W. Beck, T. Xu, J.B. Nicholas, J.F. Haw, J. Am. Chem. Soc. 117 (1995) 11594.
[77] A. Corma, G. Sastre, R. Viruela, J. Mol. Catal. A 100 (1995) 75.
[78] M.V. Frash, V.N. Solkan, V.B. Kazansky, J. Chem. Soc., Faraday Trans. 93 (1997) 515.
[79] J.F. Haw, B.R. Richardson, I.S. Oshiro, N.L. Lazo, J.A. Speed, J. Am. Chem. Soc. 111 (1989) 2052.
[80] T. Tao, G.E. Maciel, J. Am. Chem. Soc. 117 (1995) 12889.
[81] T. Xu, D.H. Barich, P.W. Goguen, W. Song, Z. Wang, J.B. Nicholas, J.F. Haw, J. Am. Chem. Soc. 120 (1998) 4025.
[82] P.H.J. Espeel, K.A. Vercruysse, M. Debaerdemaker, P.A. Jacobs, Stud. Surf. Sci. Catal. 84 (1994) 1457.
[83] G.A. Russell, J. Am. Chem. Soc. 81 (1959) 4834.
[84] G.A. Olah, J.A. Olah, T. Ohyama, J. Am. Chem. Soc. 106 (1984) 5284.
[85] Z. Zhou, R.G. Parr, J. Am. Chem. Soc. 112 (1990) 5720.